Temperature dependence of the low-frequency magnetic excitations in USb

M. Hagen* and W. G. Stirling†
Solid State Division, Oak Ridge National Laboratory, Oak Ridge, Tennessee 37831-6061

G. H. Lander
Argonne National Laboratory, Argonne, Illinois 60439-4843
and European Institute for Transuranium Elements,‡ Postfach 2340, D-7500 Karlsruhe 1, Federal Republic of Germany
(Received 7 July 1987)

The low-frequency inelastic magnetic response in the type-I fcc antiferromagnet uranium antimonide (USb) has been studied by inelastic neutron scattering in the temperature range from 12 K ($0.06T_N$) up to 320 K ($1.51T_N$). At the lowest temperature, the lowest-lying magnetic excitations in USb are a well-defined, dispersive, spin-wave branch. In the temperature range up to 100 K, the principal effect of temperature on this spin-wave branch is to increase the frequencies of the spin waves. However, in the temperature range from 100 to 160 K, these spin waves become progressively damped until at 160 K ($0.75T_N$) they have collapsed into broad inelastic scattering that peaks only at zero frequency. This scattering is a precursor to the critical scattering which develops around the Néel temperature of $T_N = 212.30 \pm 0.05$ K. The critical scattering both above and below the Néel temperature has been measured and the critical exponents and amplitude ratios associated with the inverse correlation lengths, the staggered susceptibility, and the characteristic frequency have been determined. These exponents are discussed in terms of a system in a $d = 3$, $n = 3$ universality class. In the temperature range above T_N, precursor critical scattering has been observed up to 320 K ($\sim 1.5T_N$).

I. INTRODUCTION

Although the accumulated knowledge of the magnetic properties of the actinides and their compounds is still small when compared with that of the transition metals and the rare earths, there has been considerable interest in these properties,[1] especially in recent years. A group of actinide compounds which has aroused particular interest is the UX series, where X is either a pnictide (X =N, P, As, Sb, or Bi) or a chalcogenide (X =S, Se, or Te). In this paper we report a quantitative study of the temperature dependence of the low-frequency magnetic excitations in one of these UX compounds, uranium antimonide (USb). The range of temperatures covered is from 12 K ($0.06T_N$), where the low-frequency excitations are spin waves, up to the Néel temperature, $T_N = 212.3$ K, where the low-frequency excitations peak only at zero frequency, and above T_N up to 320 K ($1.5T_N$).

The format of this paper is as follows. In the next section the functions we have used to fit the inelastic magnetic response at various temperatures are described and then in the third section the experimental conditions under which the measurements were performed are described. The experimental results are presented in the fourth section and a discussion of these results is given in the fifth section. Finally, in Sec. VI a summary of our results and conclusions is given.

All of the UX series of compounds have the fcc NaCl crystal structure at high temperature. At low temperature the chalcogenides all order ferromagnetically, whereas the pnictides are all antiferromagnets. The size of the ordered magnetic moment at low temperature and the transition temperature in the UX series can be correlated with the size of the lattice parameter.[2,3] In UN, UP, and UAs the transition from the paramagnetic state is to a type-I single-**k** structure with the magnetic moment parallel to **k** which is one of the equivalent (1,0,0) directions.[2] The transition in UN is second order and the single-**k** state remains stable down to low temperatures, whereas in UP and UAs the transition from the paramagnetic state is first order and both compounds undergo a further first-order transition at lower temperature. The magnetic structure of USb was initially thought to be a single-**k** type-I structure as in UN. However, the measurement of the low-temperature spin waves in USb by Lander *et al.*[4] showed that if such a structure were assumed then the low-frequency spin waves had a longitudinal polarization rather than the usual transverse polarization. Subsequent to these measurements it was pointed out by Jensen and Bak[5] that the observed polarization of the spin waves could alternatively be explained as transverse excitations in a triple-**k** type-I structure, in which the magnetic moments are along the (1,1,1) directions.

For clarity the single-**k** and triple-**k** structures are shown in Figs. 1(a) and 1(b), respectively. For a multidomain crystal the neutron diffraction pattern for these two structures is the same. However, this domain degeneracy can be broken by the application of uniaxial pressure along a (1,0,0) crystal axis, which for the single-**k** structure preferentially favors one domain. This

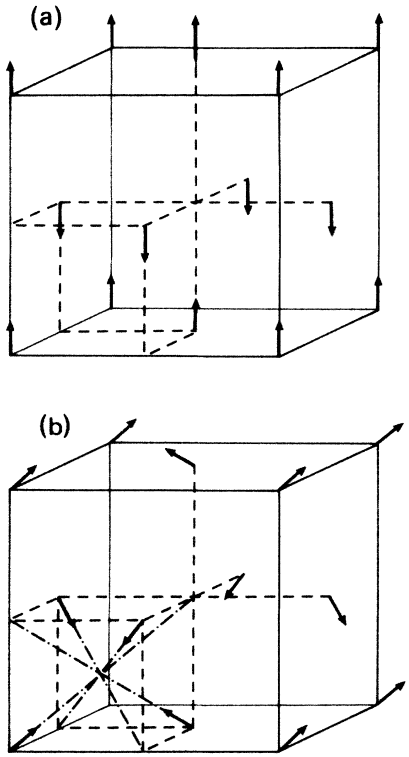

FIG. 1. The magnetic structures of the type-I fcc antiferromagnet with a single-**k** of (1,0,0) and a triple-**k** of (1,0,0) are shown in (a) and (b), respectively.

effect was used by Rossat-Mignod *et al.*[2,6] to determine the magnetic structures of a number of uranium pnictides, including USb which was indeed found to have a triple-**k** structure at all temperatures below the Néel temperature.

The measurements of Lander *et al.*[4] showed that the low-temperature inelastic magnetic response in USb for frequencies below 7 THz consisted of two spin-wave branches, a sharp lower branch which rose steeply in frequency from 1.5 THz at the magnetic zone center up to about 6 THz, and a higher, relatively dispersionless, branch which ranged in frequency from 6 to 7 THz. The existence of sharp, well-defined low-temperature spin waves in USb is unique amongst the U*X* compounds; the only other compound with any well-defined low-temperature spin waves is UTe,[3] in which the spin waves are only sharp close to the zone center. In the other U*X* compounds UN (Ref. 7), UAs (Ref. 8), US (Ref. 3), and USe (Ref. 9) the low-frequency inelastic magnetic spectra are all dominated by a broad Lorentzian line shape, centered on zero frequency. However, in UN and US broad, but weak excitations have also been observed which peak at nonzero frequency, although only at low temperature and close to the zone center.

It has been suggested by Buyers and Holden[3] that this absence of spin waves in some of the U*X* compounds can be explained by an interaction between the localized magnetic 5*f* electrons and the 6*d* conduction electrons which leads to a damping of the spin waves. In such a model the existence of sharp spin waves in USb and UTe at low temperature correlates with their being less metallic than the other compounds. Recently, Halg and collaborators[10] have repeated the earlier low-temperature spin-wave measurements for USb and, using ordinary crystal-field theory with an anisotropic form for the exchange interaction, but no *f-d* coupling interaction, were able to fit the observed dispersion relations, albeit with a large number of exchange parameters.

The object of the present study has been firstly to examine the temperature dependence of the low-frequency spin waves in USb. The earlier work of Lander *et al.*[4] suggested that at higher temperatures the well-defined spin waves disappeared and that the inelastic magnetic response then resembled that of systems such as UN (Ref. 7) and US (Ref. 3). However, the earlier work was inconclusive concerning the particular mechanism which caused this disappearance, whether "extra" low-frequency scattering obscured the discrete excitation or whether the spin wave simply became highly damped. Secondly, the critical scattering in USb (Ref. 11) shows interesting anisotropic behavior, which has been interpreted in this and other systems[2] as a consequence of anisotropy in the *longitudinal* susceptibility. Since the spin waves in USb are a *transverse* response[5] our interest is in how this evolves and interacts with the supposedly longitudinal response that is very strong near T_N. Finally, for a complete understanding of these U*X* systems, theories such as those involving anisotropic exchange parameters[10] or more microscopic ones involving anisotropy arising from hybridization[12] must be able to account for the temperature dependence of the magnetic response.

II. THEORETICAL BACKGROUND

In this section the functions that we have used to fit the experimental data are briefly described. Apart from an overall scale factor the measured neutron inelastic scattering spectrum is given by the convolution of an instrumental resolution function with the dynamic structure factor describing the inelastic magnetic properties of the sample, $S(\mathbf{Q},\omega)$.

The dynamic structure factor is given in terms of the imaginary part of the dynamic susceptibility $\chi(\mathbf{Q},\omega)$ through the relation,[13]

$$S(\mathbf{Q},\omega)=\sum_{\alpha,\beta}\left[\delta_{\alpha\beta}-\frac{Q_\alpha Q_\beta}{Q^2}\right][1+n(\omega)]\mathrm{Im}[\chi^{\alpha\beta}(\mathbf{Q},\omega)]\ , \tag{1}$$

where $\mathbf{Q}$ is the wave-vector transfer, ω is the frequency transfer, $n(\omega)$ is the Bose population factor, and the indices α and β run over the Cartesian coordinates x,y,z. In its turn the imaginary part of the dynamic susceptibility is given in terms of the static susceptibility $\chi(\mathbf{Q})$ and the spectral weight function $F(\mathbf{Q},\omega)$ through the equation[13]

$$\mathrm{Im}[\chi^{\alpha\beta}(\mathbf{Q},\omega)]=\chi^{\alpha\beta}(\mathbf{Q})\omega F^{\alpha\beta}(\mathbf{Q},\omega)\ . \tag{2}$$

In the experimental results section it will be shown that at each temperature only one function is needed to

describe the observed inelastic scattering, and therefore we will drop the polarization indices α and β. Furthermore, since only the low-frequency spin-wave branch in USb has been studied, reference to spin-wave frequencies, etc. will implicitly refer to this low-frequency branch. The explicit choice of function depends on the temperature range in which the measurements were performed. At low temperatures the choice of function is related to a spin-wave model, whereas at higher temperatures, around T_N, the choice of function is given by the theory of critical phenomena.

The function chosen to fit the data at lower temperatures ($T \leq 170$ K) was the damped-harmonic-oscillator (DHO) function which is given by

$$F(\mathbf{Q},\omega)=\frac{1}{\pi}\frac{\Omega^2(\mathbf{q})\alpha(\mathbf{q})}{[\omega^2-\Omega^2(\mathbf{q})]^2+\omega^2\alpha^2(\mathbf{q})} , \tag{3}$$

where $\mathbf{q}=\mathbf{Q}-\tau$ and τ is the magnetic zone center.

This function has been used very successfully by a number of authors to describe the temperature dependence of spin-wave line shapes in both ferromagnets[14] and antiferromagnets.[15] It is normal to associate the parameter $\Omega(\mathbf{q})$ with the intrinsic spin-wave frequency and the parameter $\alpha(\mathbf{q})$ with the spin-wave damping. In the limit that $\alpha(\mathbf{q})$ goes to zero, Eq. (3) reduces to the difference of two δ functions with $\Omega(\mathbf{q})$ being the low-temperature dispersion relation. However, if the spin-wave damping $\alpha(\mathbf{q})$ in Eq. (3) is not small compared to the intrinsic frequency $\Omega(\mathbf{q})$ then the frequencies at which $S(\mathbf{Q},\omega)$ peaks do not correspond to $\Omega(\mathbf{q})$. Instead, these frequencies correspond, to a good approximation, to the frequencies $\pm\omega_p(\mathbf{q})$ at which the function $F(\mathbf{Q},\omega)$ peaks. The frequency $\omega_p(\mathbf{q})$ is given by

$$\omega_p(\mathbf{q})=[\Omega^2(\mathbf{q})-\tfrac{1}{2}\alpha^2(\mathbf{q})]^{1/2} . \tag{4}$$

Therefore, if $\alpha(\mathbf{q})>\sqrt{2}\Omega(\mathbf{q})$ then $S(\mathbf{Q},\omega)$ only peaks at zero frequency.

In the critical region we have used a Lorentzian form for the spectral weight function $F(\mathbf{q},\omega)$ given by

$$F(\mathbf{q},\omega)=\frac{1}{\pi}\frac{\Gamma(\mathbf{q})}{\omega^2+\Gamma^2(\mathbf{q})} , \tag{5}$$

where $\Gamma(\mathbf{q})$ is the wave-vector-dependent characteristic frequency, and a Lorentzian form for the staggered static susceptibility $\chi(\mathbf{q})$ given by

$$\chi(\mathbf{q})=\frac{\chi(\mathbf{0})}{1+(q_x/K_x)^2+(q_y/K_y)^2+(q_z/K_x)^2} , \tag{6}$$

where K_x and K_y are inverse correlation lengths. The directions x, y and z are defined to be the orthogonal directions [1,1,0], [0,0,1], and [1,$\bar{1}$,0], respectively. In the theory of critical phenomena the characteristic frequency is proportional to the inverse of the static staggered susceptibility,[16] i.e., $\Gamma(\mathbf{q})\propto\chi^{-1}(\mathbf{q})$. A slightly more general form for $\Gamma(\mathbf{q})$ was used to fit the experimental data given by

$$\Gamma(\mathbf{q})=\Gamma(\mathbf{0})[1+(q_x/K_x)^2+(q_y/K_y)^2+(q_z/K_x)^2] \tag{7}$$

This more general form has been used very successfully to model the dynamic critical scattering chromium[17] and uranium nitride[18] (the latter of which is closely related to USb), and is applicable to both Ising[19] and Heisenberg[20] antiferromagnets.

III. EXPERIMENTAL DETAILS

All of the measurements reported in this paper were performed at the High Flux Isotope Reactor, Oak Ridge National Laboratory, using the HB-2 and HB-3 triple-axis spectrometers. In order to perform the various scans at different temperatures these spectrometers were operated with differing wave-vector and frequency resolutions in the different temperature ranges, depending upon the strength of the observed signal. The variation in resolution was governed by varying the fixed final neutron frequency (E_f) in the scattering process with the other parameters describing the spectrometer configurations essentially unchanged. These constant parameters will be described first, followed by the differences for each of the temperature ranges in which the scattering was measured.

The monochromators and analyzers used were the {0,0,2} planes of pyrolytic graphite crystals. The collimation used was 120′ before the monochromator, 40′ monochromator to sample and sample to analyzer, and 120′ from analyzer to detector. In order to help focus the spin waves at low temperature, the spectrometers were operated in the *W* configuration, and where appropriate the spin waves were always measured in the position which was focused for neutron frequency-loss scattering.

The measurements of the spin-wave scattering and the precursor critical scattering below T_N and the precursor scattering at 320 K were measured with a value of $E_f=6$ THz. For the temperature range between 209 and 219 K where the critical scattering was measured, a value of $E_f=1.087$ THz was used. In this configuration a 7-cm-long piece of polycrystalline beryllium was placed in the incident beam before the monitor to filter out neutrons scattered from higher-order planes in the monochromator. The measurements of the precursor critical scattering above T_N from 235 to 280 K were performed with $E_f=3.6$ THz and a pyrolytic graphite filter between the sample and analyzer.

The sample of USb used was a single crystal of volume 0.3 cm^3, grown by O. Vogt and K. Mattenberger at the Eidgenössische Technische Hochschule (ETH), Zurich, Switzerland. We note that this detailed line-shape analysis was made possible by the growth of a large single crystal; previous work[4] employed a less-well-oriented array of several crystals. This crystal was aligned with a [1,1,0] axis vertical and mounted in an aluminum can with a helium exchange gas atmosphere. The aluminum can was attached to the cold tip of a Displex refrigerator which was controlled with a Cryocal T-2000 temperature controller. A calibrated silicon diode in the sample can was used to measure the sample temperature over the whole range of temperatures studied.

IV. EXPERIMENTAL RESULTS

The experimental results presented in this section have been organized into four subsections, each representing a different qualitative aspect of the observed inelastic magnetic response. Firstly, the results for temperatures $T \leq 170$ K, which we refer to as the spin-wave regime because $S(Q,\omega)$ can be described well by a spin-wave model, are presented. For temperatures $T > 170$ K the observed inelastic magnetic response is best described by a "critical scattering" model. The theory of critical phenomena predicts quantitative results (i.e., critical exponents) only for a narrow temperature range around the transition temperature, and as a consequence we have only used data in the temperature range $209 < T < 219$ K, where high-resolution measurements were performed, for a quantitative analysis of the critical region. The results for this temperature range are reported in the second subsection. The remaining two subsections report the results of measurements of what we refer to as the precursor critical scattering. This is scattering whose form is qualitatively that of critical scattering, but which occurs in a temperature range which would conventionally be expected to be outside the critical region where critical exponents could be extracted. In the first of these two subsections the results for the temperature range $180 < T < 205$ K, which connects the spin-wave and critical regimes are presented, and then in the final subsection the results in the temperature range $235 < T < 320$ K, above the transition temperature, are briefly described. Clearly, the boundaries between these four temperature ranges cannot be distinct and our choice of the particular temperatures of these boundaries has been dictated by the practical need to change the spectrometer configuration in order to be

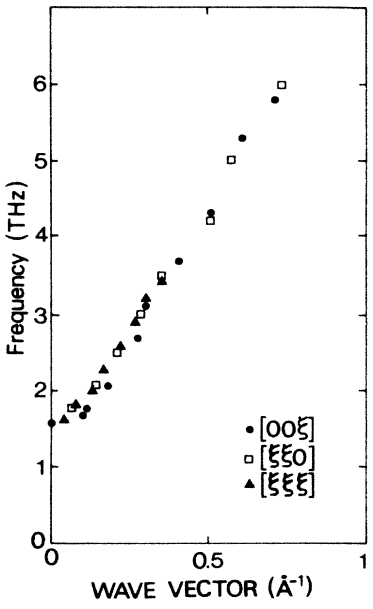

FIG. 2. Measured spin-wave frequencies in USb for the [0,0,ξ] and [ξ,ξ,0] directions (Ref. 7) and in the [ξ,ξ,ξ] direction (this work). (1 THz≡4.14 meV=48 K.)

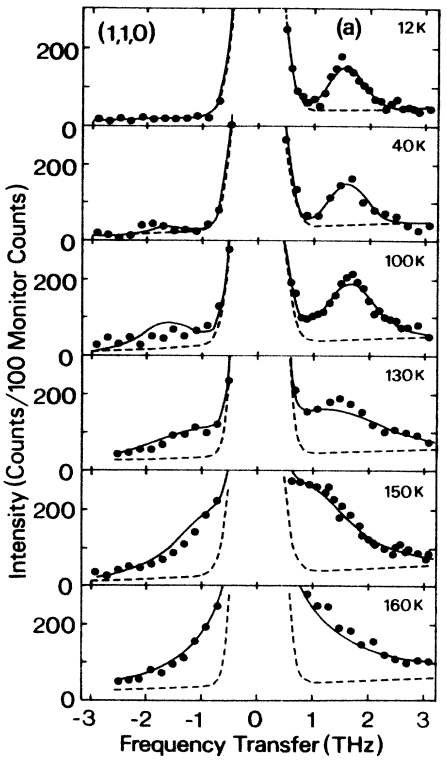

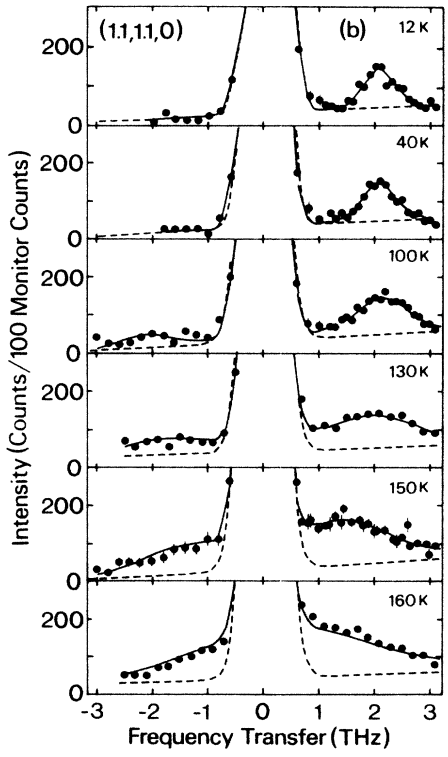

FIG. 3. The temperature dependence of the low-frequency magnetic response is shown at the wave vectors (1,1,0) and (1.1,1.1,0) on (a) and (b), respectively. The solid lines are fits to the data as discussed in the text, and the dashed lines represent the background scattering.

able to perform the relevant measurements in each temperature range. The question of the size of the critical region and hence the distinction between critical and precursor critical scattering is discussed further in Sec. V in light of the experimental results.

A. Spin-wave regime

In the previous measurements of the low-temperature spin waves in USb,[4,10] the dispersion relation of the low-frequency branch in the $[\xi,\xi,\xi]$ direction had not been measured. For completeness we have measured this dispersion relation as a preliminary before studying the temperature dependence of the spin waves; it is shown in Fig. 2, along with the earlier measurements[4] along $[\xi,\xi,0]$ and $[0,0,\xi]$. We note that the spin-wave dispersion relation is isotropic at low temperature.

The temperature dependence of the spin waves in USb was measured at five wave vectors close to the (1,1,0) antiferromagnetic Bragg position. These wave vectors were (1,1,0.2), (1,1,0.1), (1,1,0), (1.1,1.1,0), and (1.2,1.2,0). In Figs. 3(a) and 3(b), inelastic scans at the wave vectors (1,1,0) and (1.1,1.1,0), respectively, are shown at various temperatures in the range from 12 to 160 K. The low-temperature scans at $T=12$ K show sharp well-defined spin-wave peaks in good agreement with previous measurements.[4,10] The solid lines in Figs. 3 for the $T=12$-K data are fits to Gaussian line shapes for the spin waves, a Gaussian form for the incoherent nuclear scattering at zero frequency and a sloping background. The initial effect of temperature on these spin waves is to *increase* the spin-wave frequency, which can be seen from an inspection of the $T=40$-K data in Figs. 3(a) and 3(b). This effect was noted previously by Lander and coworkers.[4] This increase in frequency continues up to a temperature somewhere between 80 and 100 K, where the spin waves become noticeably damped. Above 100 K the damping of the spin waves increases rapidly, and at 130 K the frequency at which the scattering peaks has shifted downwards from its 100-K value and the scattering is broad in frequency. At 150 K it is just possible to discern peaks in the scattering at nonzero frequency, but by 160 K the scattering function peaks only at zero frequency.

To quantify these changes in the spin-wave spectrum we have fitted the experimentally measured spin-wave spectra for $T>12$ K to the DHO function given in Eq. (3) convoluted with the instrumental resolution function and the temperature population factor. Also included in these fits for $T>12$ K were a Gaussian form for the incoherent scattering and a sloping background which were determined at low temperature (12 K) and held fixed at higher temperatures. The resulting fits are shown for $T>12$ K by the solid lines of Figs. 3.

The principal fitting parameters in Eq. (3) are the intrinsic spin-wave frequency $\Omega(\mathbf{q})$ and the spin-wave damping $\alpha(\mathbf{q})$. In Figs. 4(a) and 4(b) the temperature dependence of the values of $\Omega(\mathbf{q})$ and $\alpha(\mathbf{q})$ are shown for the five wave vectors studied. Also shown, in Fig. 4(c), is the temperature dependence of the frequency at which the scattering peaks, $\omega_p(\mathbf{q})$, given by Eq. (4). The solid lines in Figs. 4(a) and 4(c) are merely guides to the eye, although the data is perhaps suggestive of a linear temperature dependence for $\Omega(\mathbf{q})$. The values of $\alpha(\mathbf{q})$, the spin-wave damping, are not particularly well defined below 100 K where the absolute values are small. The overall temperature dependence of $\alpha(\mathbf{q})$ appears to be roughly the same at all five wave vectors, with a rapid increase between 100 and 160 K.

At 160 K, and at 170 K where data were also taken, it is possible to fit the inelastic spectra to a Lorentzian line shape [cf. Eq. (5)]. A comparison between the DHO and Lorentzian fits to the data at these temperatures shows little if any significant difference in the quality of fit given by the two functions. It is well known that the DHO and Lorentzian functions are very similar when the scattering only peaks at zero frequency. The characteristic frequency of the Lorentzian $\Gamma(\mathbf{q})$ is then approximately related to the $\Omega(\mathbf{q})$ and $\alpha(\mathbf{q})$ parameters of the DHO by the relation $\Gamma(\mathbf{q})=\Omega^2(\mathbf{q})/\alpha(\mathbf{q})$. In Table I the fitted parameters of the DHO function, $\Omega(\mathbf{q})$, $\alpha(\mathbf{q})$, $\Omega^2(\mathbf{q})/\alpha(\mathbf{q})$, and $\Gamma(\mathbf{q})$ for the Lorentzian are listed. As can be seen from Table I the two functions give very similar characteristic frequencies and hence similar descriptions of the observed scattering.

It should be emphasized that below 150 K the spin-wave scattering cannot be fitted by a Lorentzian line shape since it has peaks at nonzero frequency. Furthermore, there is no need below 150 K for a Lorentzian plus DHO to fit the data; the scattering can be completely described by a DHO function alone. Attempts to include a Lorentzian (centered on zero frequency) as well as a DHO in the fitting function for temperatures below 150 K lead to an unacceptably small amplitude for the Lorentzian.

A Lorentzian peak centered on zero frequency is characteristic of magnetic critical scattering, and the collapse of the spin-wave scattering into such a peak leads to the speculation that this scattering develops into the critical scattering. To examine this question we have also studied the critical scattering in the USb both above and below the Néel temperature, and the scattering in

TABLE I. The results for the fitting parameters Ω and α for the DHO function, and Γ for the Lorentzian function, are tabulated for the data taken at 160 K, along with the combination Ω^2/α.

Wave vector	Ω (THz)	α (THz)	Ω^2/α (THz)	Γ (THz)
(1.1,−0.2)	2.13±0.20	3.32±0.15	1.37±0.26	1.28±0.16
(1.1,−0.1)	1.76±0.15	3.30±0.28	0.94±0.18	0.86±0.12
(1,1,0)	1.81±0.15	3.57±0.10	0.92±0.16	0.84±0.12
(1.1,1.1,0)	2.32±0.31	4.03±0.64	1.34±0.47	1.38±0.12
(1.2,1.2,0)	3.21±0.17	4.60±0.40	2.24±0.31	2.73±0.27

the precursor critical region between 170 K and the critical region.

B. Critical regime

The frequency-integrated critical scattering in USb has been measured previously, above the Néel temperature, by Lander *et al.*[11] In the measurements reported here, we have studied the frequency dependence of the critical scattering, as well as its wave-vector dependence at temperatures both above and below the Néel temperature. These measurements were performed at five temperatures above the Néel temperature and four below, and consisted of a series of elastic and inelastic scans through and near the magnetic zone center (1,1,0). These sets of data were fitted to Eqs. (5)–(7) convoluted with the resolution function of the spectrometer. The resolution function was described using the formalism of Cooper and Nathans[21] in which each component of the spectrometer is assumed to have a Gaussian transmission function with an effective full width at half maximum (FWHM). A set of effective FWHM which reproduced

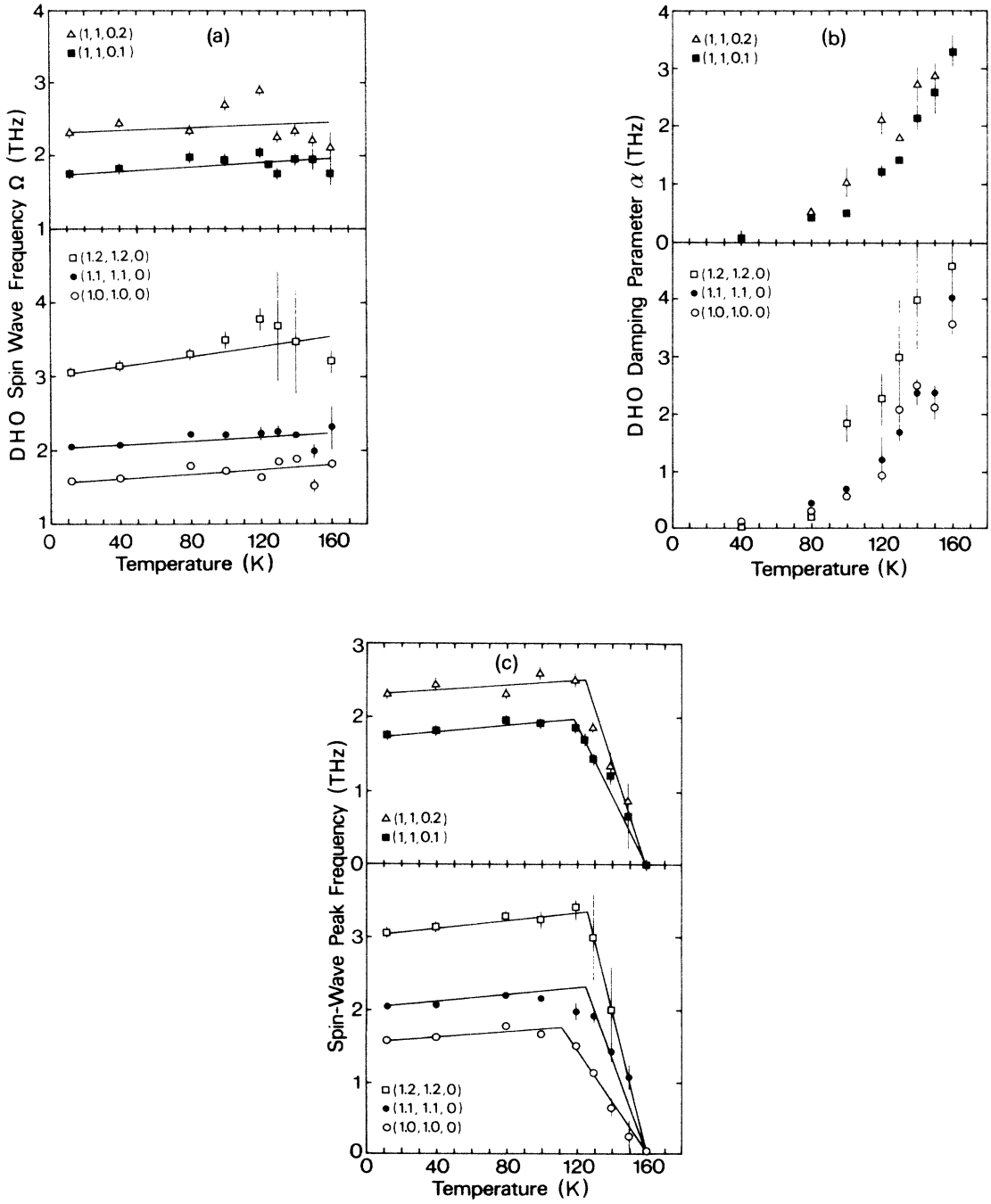

FIG. 4. The temperature dependence of the parameters $\Omega(\mathbf{q})$, $\alpha(\mathbf{q})$, and $\omega_p(\mathbf{q})$ deduced from the fits to a damped-harmonic-oscillator line shape described in the text are shown in (a), (b), and (c), respectively. The solid lines are guides to the eye.

TABLE II. The effective collimation (FWHM) parameters used to describe the instrumental resolution function (Ref. 21) are tabulated (α and β are effective horizontal and vertical collimations, respectively, while the η values represent the relevant mosaic spreads), along with the measured resolution widths at (1,1,0).

Instrumental parameters; effective collimation (FWHM)			
$\alpha_1=120'$	$\alpha_2=52'$	$\alpha_3=52'$	$\alpha_4=120'$
$\beta_1=229'$	$\beta_2=146'$	$\beta_3=158'$	$\beta_4=442'$
$\eta_M=26'$	$\eta_S=10'$	$\eta_A=26'$	

	Measured resolution widths (FWHM) at (1,1,0)			
E_f (THz)	Transverse (Å^{-1})	Longitudinal (Å^{-1})	Vertical (Å^{-1})	Frequency (THz)
1.097	0.008	0.013	0.083	0.0093
6.00	0.008	0.030	0.200	0.023

the measured FWHM of the (1,1,0) Bragg peak were determined and are listed in Table II, with the measured widths. In Figs. 5(a) to 5(c) some of the data taken at 210.2 K (below T_N) and 215.2 K (above T_N) are shown along with the fitted curves. At each temperature the fitting procedure led to values of $K_x(T)$, $K_y(T)$, $\Gamma(\mathbf{0},T)$, and $\chi(\mathbf{0},T)$ which were defined in Eqs. (6) and (7). In Figs. 6(a) to 6(d) the values of $K_y(T)$, $K_x(T)$, $\Gamma(\mathbf{0},T)$, and $[\chi(\mathbf{0},T)]^{-1}$ determined in this way are presented. It is worth commenting on the values of $\Gamma(\mathbf{0},T)$ determined from the fitting procedure. These values are small compared to the resolution of the spectrometer, whereas the actual frequency widths of the scattering measured were larger than the resolution. This effect arises because of the large size of the terms which scale with the inverse correlation lengths in Eq. (7) when integrated over the resolution function. The values for $K_x(T)$, $K_y(T)$, $\Gamma(\mathbf{0},T)$, and $\chi(\mathbf{0},T)$ have been fitted to power-law functions of the reduced temperature $t=(T-T_N)/T_N$, given by

$$K_x(T)=K_x^{\pm}\,|\,t\,|^{\nu_x}\,, \tag{8a}$$

$$K_y(T)=K_y^{\pm}\,|\,t\,|^{\nu_y}\,, \tag{8b}$$

$$\Gamma(\mathbf{0},T)=\Gamma^{\pm}(\mathbf{0})\,|\,t\,|^{\Delta}\,, \tag{8c}$$

$$\chi(\mathbf{0},T)=\chi^{\pm}(\mathbf{0})\,|\,t\,|^{-\gamma}\,, \tag{8d}$$

where ν_x, ν_y, Δ, and γ are the critical exponents which have been assumed to be the same above and below T_N, and $K_x^{\pm}$, $K_y^{\pm}$, $\Gamma^{\pm}(\mathbf{0})$, and $\chi^{\pm}(\mathbf{0})$ are the critical amplitudes above (+) and below (−) the Néel temperature. The initial fits to Eqs. (8) produced values for the Néel temperature which differed by less than 0.05 K, and consequently the fits were repeated but with T_N fixed at its average value of 212.30±0.05 K. In Table III the critical exponents and amplitudes which resulted from these latter fits are given. These best-fit power-law functions are shown in Figs. 6(a) to 6(d) by the solid lines. In the discussion section the values of the critical exponents and amplitudes will be discussed in detail and compared with those obtained for UN by Holden *et al.*[18]

C. Precursor critical regime ($T<T_N$)

In the high-resolution configuration used to study the critical scattering around the Néel temperature, the measurable signal becomes small below about 209 K. Therefore, in order to measure the scattering at temperatures intermediate between the collapse of the spin-wave scattering at 160 K and the onset of the critical scattering at 209 K, measurements were performed with a final neutron frequency of 6 THz. This configuration has a much lower instrumental resolution but, as a consequence, a much larger measured signal. The scans performed in this temperature range were similar to those performed just below the Néel temperature but over wider ranges. The temperatures considered were 180, 190,

TABLE III. The critical amplitudes and critical exponents for the inverse correlation lengths K_x and K_y, the staggered static susceptibility $\chi(\mathbf{0})$, and the characteristic frequency $\Gamma(\mathbf{0})$. Also given in the table is the ratio of the critical amplitude above T_N to those below T_N. The Néel temperature is $T_N=212.30\pm0.05$ K.

Parameter	Amplitude ($T>T_N$)	Amplitude ($T<T_N$)	Exponent	Amplitude ratio
$K_x(2\pi/a)$	0.206±0.020	0.266±0.033	0.717±0.044 (ν_x)	0.77±0.12
$K_y(2\pi/a)$	1.000±0.041	1.085±0.060	0.663±0.050 (ν_y)	0.92±0.06
$\chi(\mathbf{0})$ (arb.)	0.090±0.021	0.034±0.008	1.737±0.147 (γ)	2.65±0.88
$\Gamma(\mathbf{0})$ (THz)	1.037±0.545	0.916±0.571	1.592±0.196 (Δ)	1.13±0.92

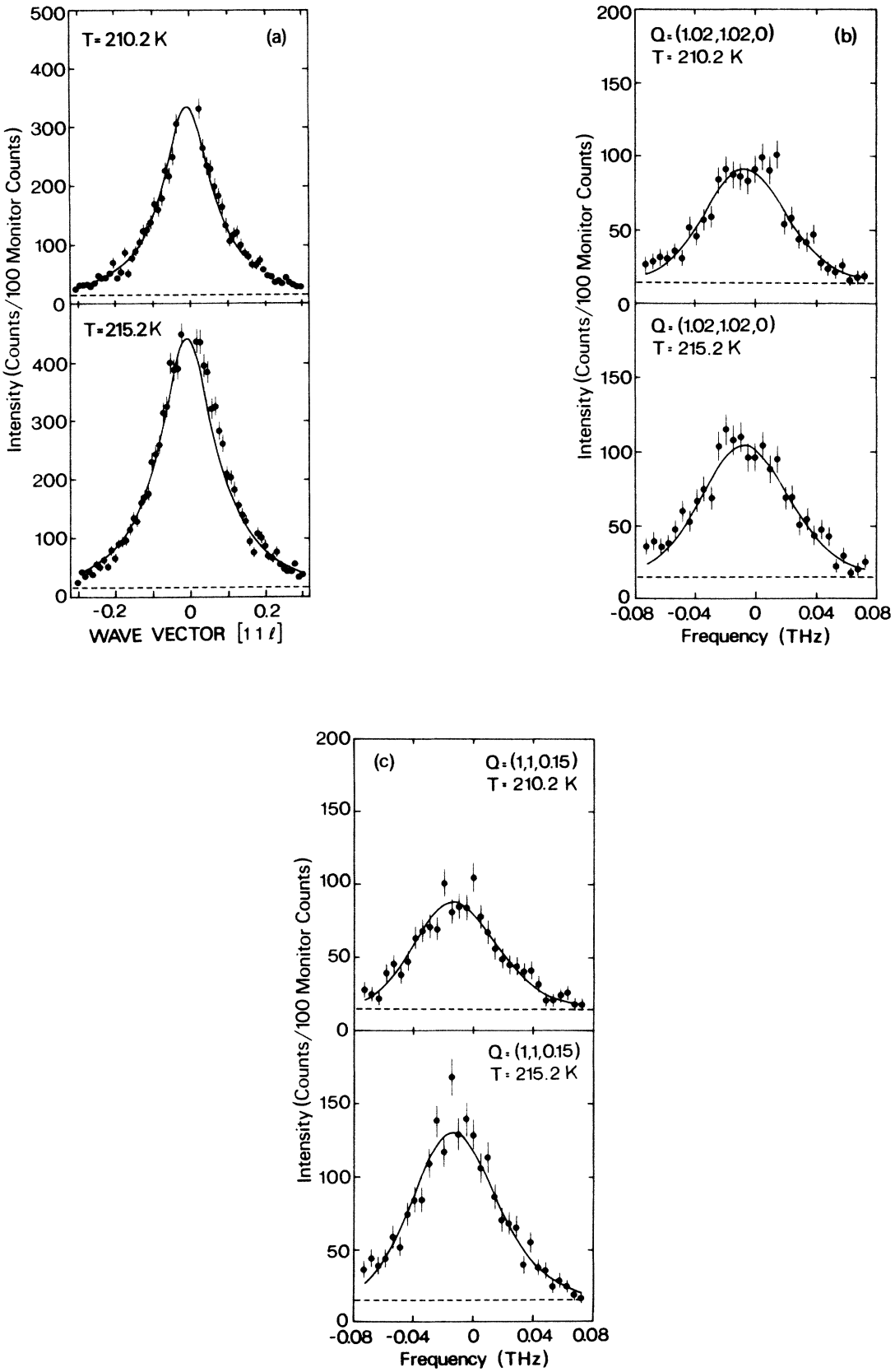

FIG. 5. A selection of the intensity distributions used to fit the critical scattering for temperatures of 210.2 K (below T_N) and 215.2 K (above T_N). (a) Wave-vector scans through (1,1,0); (b) frequency scans at (1.02,1.02,0); (c) frequency scans at (1,1,0.15). The solid lines are the results of the fits described in the text and the dashed lines are the background level. In (a) the Bragg peak scattering at (1,1,0) which occurs at 210.2 K has been deleted for clarity.

200, 205, and 12 K to determine the background level. The measured scattering distributions were analyzed in the same way as the critical scattering. The set of effective parameters used to describe the resolution function and the measured widths are given in Table II. In Figs. 7(a)–7(c) some of the 190-K measurements are shown along with the fit result given by the solid line and the background level given by the dashed line. The background levels in these scans were dependent on both the wave vector and frequency transfer, but were determined at 12 K and were held fixed in the fits to the higher-temperature data. The values of $K_x(T)$, $K_y(T)$,

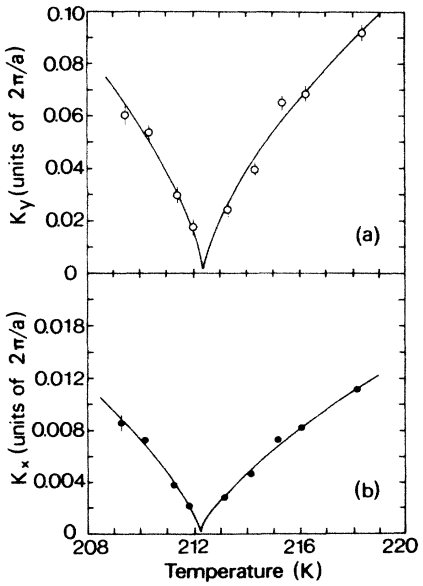

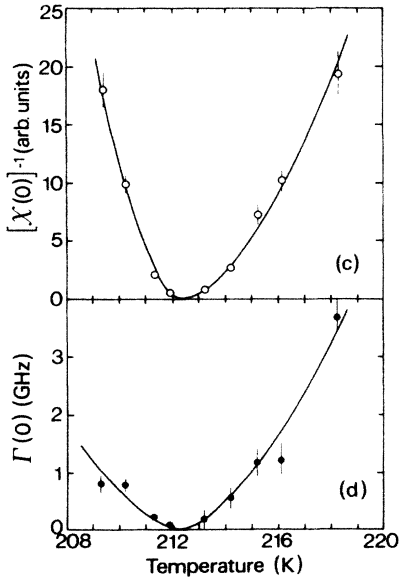

FIG. 6. The temperature dependence of the inverse correlation lengths K_y and K_x the inverse static susceptibility $[\chi(\mathbf{0})]^{-1}$ and the characteristic frequency $\Gamma(\mathbf{0})$ is shown in (a), (b), (c), and (d), respectively. The solid lines are the results of the power-law fits described in the text [Eqs. (8)].

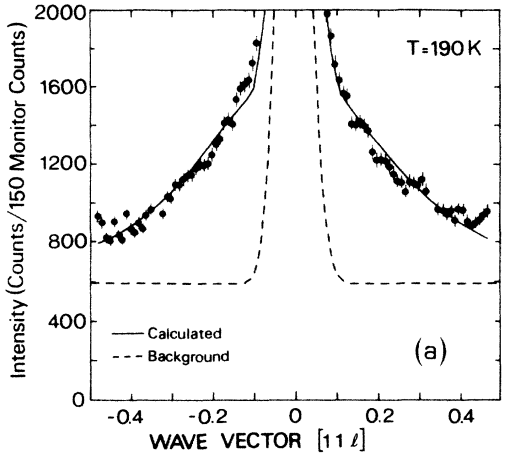

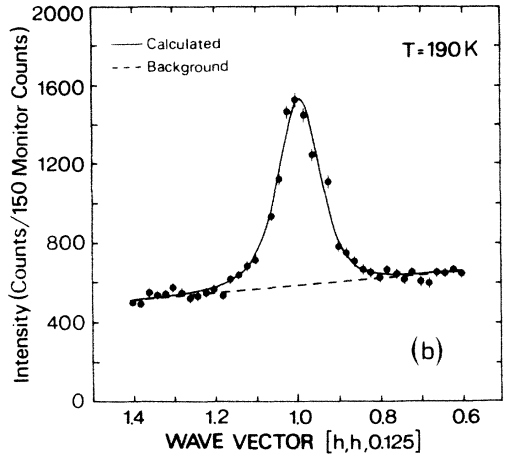

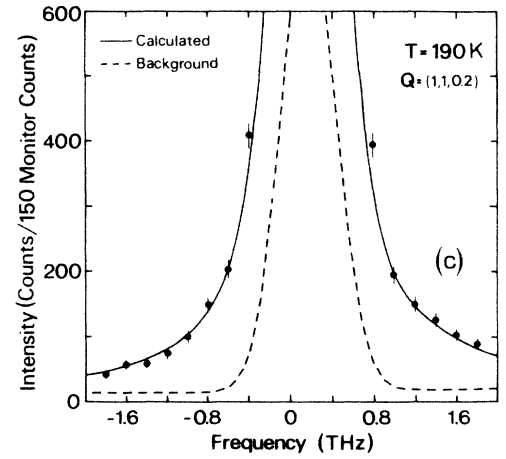

FIG. 7. A selection of the scans used in fitting the precursor critical scattering at $T=190$ K. (a) wave-vector scan through (1,1,0); (b) wave-vector scan through (1,1,0.125); (c) frequency scan at (1,1,0.2). The solid lines are the fitted functions, as described in the text, and the dashed lines represent the background including the Bragg peak and incoherent scattering.

and $\Gamma(0,T)$ determined in this way are shown in Fig. 8, along with the data from the critical region, on a log-log plot. The temperatures 180, 190, 200, and 205 K correspond to the reduced temperatures 0.152, 0.105, 0.058, and 0.034, respectively in this figure.

Figure 8 also includes values for $K_x(T)$, $K_y(T)$, and $\Gamma(0,T)$ at reduced temperatures of 0.246 and 0.199, which correspond to absolute temperatures of 160 and 170 K, respectively. These have been extracted from the values of $\Gamma(\mathbf{q})$ obtained from fitting the "spin-wave" scans at these temperatures to Lorentzians, as described in Sec. IV A. In Fig. 9 the values of the characteristic frequency $\Gamma(\mathbf{q})$ are shown for these temperatures. It should be noted that these fits have not been corrected for the effect of the wave-vector components of the resolution function, because at these temperatures K_x and K_y are large compared to the resolution widths, and such corrections should be negligible. The solid lines of Fig. 9 (and Fig. 10) represent least-squares fits to Eq. (7).

The values of K_x, K_y, and $\Gamma(0)$ shown in Fig. 8, which correspond to temperatures which range from just below the Néel temperature to just above the temperature at which the spin waves collapse, appear to fall on continuous, though nonlinear, curves. In Fig. 8, the solid lines are the power-law fits within the critical region and the dashed lines are their extrapolation outside this region. A discussion of these results will be given in Sec. V.

D. Precursor critical regime ($T > T_N$)

We present here the results of a study of the behavior of the precursor critical scattering at temperatures well above the Néel temperature. In this case also, it was necessary to increase the volume of the resolution function to obtain a measurable signal. Measurements were performed at 235, 250, and 280 K with a fixed final neutron frequency of 3.6 THz and at 320 K with a fixed final neutron frequency of 6.0 THz. The measurements at 235, 250, and 280 K were performed and analyzed in a similar way to those at 160 and 170 K. These data were fitted to Eq. (5) convoluted with the frequency resolution and the temperature factor in order to obtain values for the wave-vector-dependent characteristic frequencies $\Gamma(\mathbf{q})$. As before, these values of $\Gamma(\mathbf{q})$ were fitted to Eq. (7) in order to extract values for $K_x(T)$, $K_y(T)$, and $\Gamma(0,T)$. In Fig. 10 the values of $\Gamma(\mathbf{q})$ deter-

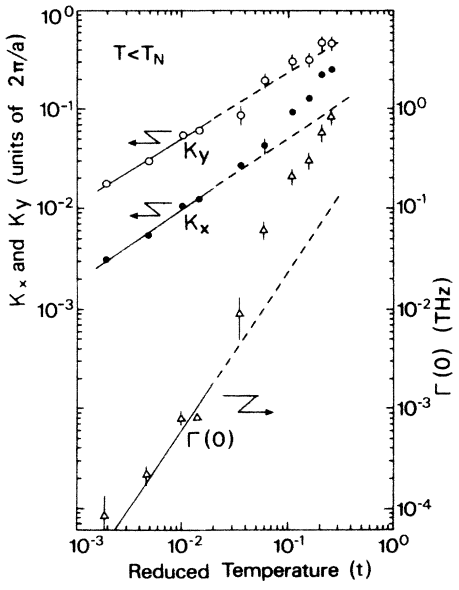

FIG. 8. A log-log plot of the inverse correlation lengths K_x and K_y and the characteristic frequency $\Gamma(0)$ against reduced temperature is shown for temperatures between 212 and 160 K ($T < T_N$). The solid lines are the fits to power-law fits within the critical region and the dashed lines the extrapolation of these fits.

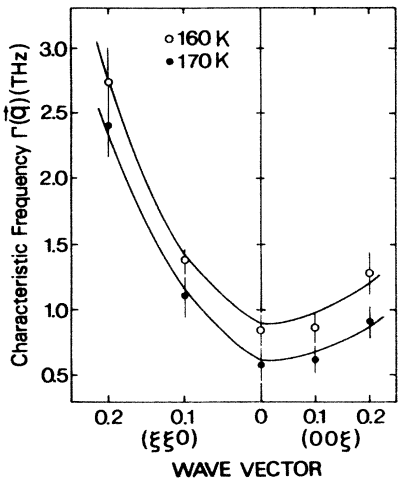

FIG. 9. The wave-vector-dependent characteristic frequencies obtained from the Lorentzian fits to the inelastic scattering data at 160 and 170 K, as described in the text. The solid lines are the fits to Eq. (7) which are described in the text.

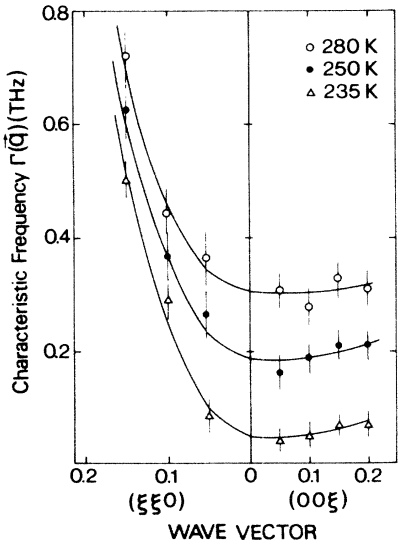

FIG. 10. The wave-vector-dependent characteristic frequencies obtained from the Lorentzian fits to the inelastic scattering data at 235, 250, and 280 K, as described in the text. The solid lines are the fits to Eq. (7) which are described in the text.

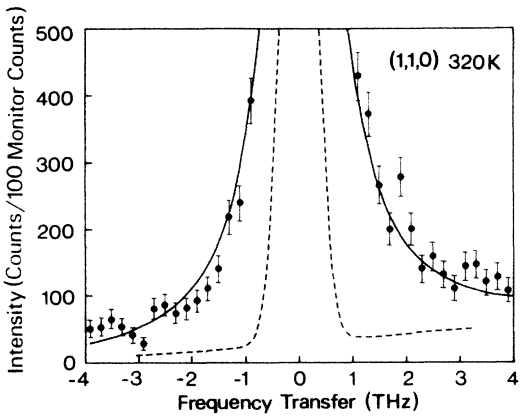

FIG. 11. A quasielastic scan at (1,1,0) at $T=320$ K ($\sim 1.5T_N$). The solid line is the result of a fit to a Lorentzian line shape and the dashed line represents the background scattering, including the incoherent contribution.

mined at these temperatures and the fits to Eq. (7) are shown for these three temperatures.

At the highest temperature considered (320 K) insufficient measurements were made to obtain meaningful values of K_x and K_y. However, even at this temperature, which is $\sim 1.5T_N$, there is still significant scattering around (1,1,0) as shown in Fig. 11. This frequency scan has been fitted as described above and the fitted function is shown by the solid line of Fig. 11. At this temperature we have assumed that the value of the characteristic frequency determined from this fit is a good estimate of $\Gamma(0,T)$ since K_x and K_y will be very large.

In Fig. 12 a log-log plot of all of the values of $K_x(T)$, $K_y(T)$, and $\Gamma(0,T)$ determined above the Néel temperature is shown. As in Fig. 8 the solid lines in Fig. 12 are the power-law fits within the critical region and the dashed lines are their extrapolation outside the critical region.

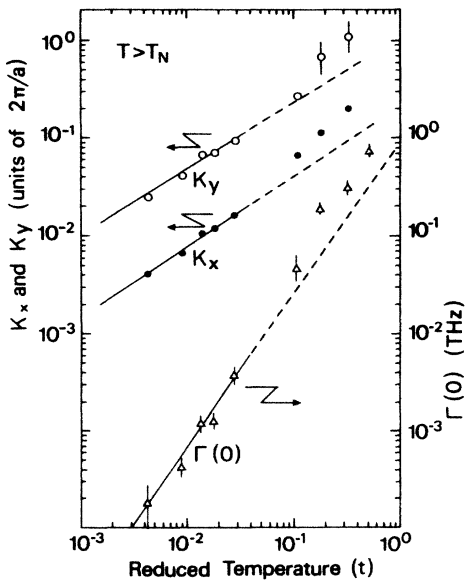

FIG. 12. A log-log plot of the inverse correlation lengths K_x and K_y and the characteristic frequency $\Gamma(0)$ against reduced temperature is shown for temperatures between 212 and 320 K ($T > T_N$). The solid lines are the power-law fits within the critical region and the dashed lines the extrapolation of these fits.

V. DISCUSSION

Qualitatively, the temperature dependence of the low-frequency magnetic response in USb may be summarized as follows. At low temperatures the low-frequency response takes the form of sharp dispersive spin-wave branches, which broaden upon heating and collapse into a broad "quasielastic" response which only peaks at zero frequency at $0.75T_N$. This broad response evolves with increasing temperature to become what is conventionally referred to as the "critical scattering" at temperatures close to T_N. At temperatures above T_N the low-frequency inelastic response persists to temperatures well above what is usually taken to be the critical region, i.e., up to at least $1.5T_N$. A quantitative analysis of these results shows a behavior that is anomalous at all temperatures.

The initial change in the spin-wave spectrum upon raising the temperature up from low temperature to ~ 80 K is that the intrinsic frequencies of the spin waves *increase* with temperature. In this temperature range the line shape of the spin waves remains relatively sharp and this increase in the intrinsic frequencies cannot be accounted for either by a change in the line shape or by the uncertainty in determining the peak position. It should be noted that this effect is not particularly large, the zone-center mode increases in frequency by only 8% in going from 12 to 80 K. Nevertheless, this effect is somewhat surprising since in most ferromagnets and antiferromagnets the initial effect of temperature is to *decrease* the spin-wave frequencies. The low-temperature spin-wave frequencies in USb are determined by the combination of a cubic crystal-field interaction, and isotropic and anisotropic exchange interactions of both antiferromagnetic and ferromagnetic sign out to at least third-nearest neighbors.[10] It is therefore conceivable that these different interactions could vary differently with temperature, leading to the unusual increase in the spin-wave frequencies.

The effects of temperature on the spin-wave line shape in the range 80–160 K are more dramatic. The data analysis, in terms of a DHO function, suggests that the collapse of the spin-wave line shape is due to a damping mechanism rather than to a softening of the intrinsic spin-wave frequencies. In fact, as can be seen from Fig. 4(a), the intrinsic frequencies of the spin waves tend to increase much as they did in the temperature range up to 80 K. A certain degree of caution is necessary when drawing such a conclusion since the DHO line shape is not the only possible choice for $F(\mathbf{Q},\omega)$. An alternative form would be the double Lorentzian function (DLF) used by Schulhof *et al.*[22] in their study of the critical dynamics of MnF_2. This function is the sum of two Lorentzians each of the same half width α_{DLF} which are centered on the frequencies $\pm\Omega_{\mathrm{DLF}}$. For the case of a

highly damped spin wave, which would apply to USb in the temperature range $130<T<160$ K, it can be shown[15] that the DHO and DLF have a very similar line shape if the parameters α_{DLF} and Ω_{DLF} are given by

$$\Omega_{\mathrm{DLF}}=(\Omega^2-\alpha^2)^{1/2} ,$$

$$\alpha_{\mathrm{DLF}}=\alpha/2 .$$

The use of the DLF form to interpret the damping of the spin waves would therefore lead to a very similar temperature dependence for the spin-wave damping constant (although its absolute value would differ by a factor of 2) but a different temperature dependence for the "intrinsic spin-wave frequency," which would soften in the temperature range $130<T<160$ K. In the absence of theoretical work on the temperature dependence of $F(\mathbf{Q},\omega)$ in antiferromagnets such as USb below T_N to guide us, we cannot decide which function provides the best interpretation. We have chosen to use the DHO for our analysis because of its use in previous measurements of spin waves over a wide temperature range[14,15] and because in the limit of zero spin-wave damping (i.e., at low temperature) it has a more transparent relationship to linear spin-wave theory than the DLF.

It should be noted that below 160 K the low-frequency magnetic response in USb can be completely described by a *single* DHO function, and there is no need for an extra (quasielastic) peak centered on zero frequency. The earlier work[4] was unable to resolve this point because of the difficulties arising from the use of an array of crystals rather than a single crystal. In studies of both UN (Ref. 7) and US (Ref. 3) it has been reported that there are *two* components to the inelastic spectrum, a broad excitation which is centered at nonzero frequency and a Lorentzian peak centered on zero frequency. It appeared in both the work on UN and US that the growth of the peak centered on zero frequency obscured the broad excitation at nonzero frequency, at higher temperatures. This is certainly not the case in USb at low frequencies and small q, as the spin-wave scattering collapses to become a Lorentzian peak centered on zero frequency.

Above 160 K the low-frequency inelastic magnetic response at small wave vector evolves continuously with temperature from the "collapsed spin waves" into the critical scattering associated with the phase transition at $T_N=212.3$ K. This evolution with temperature implies that the *transverse* magnetic susceptibility diverges at the Néel temperature, as well as the *longitudinal* magnetic susceptibility. Furthermore, since at any one temperature only *one* function is needed to describe the inelastic magnetic response, these results imply that, as a function of frequency, the longitudinal and transverse susceptibilities are very similar if not degenerate above 160 K. Previous work on UN and USb has assumed that the critical scattering and precursor critical scattering were totally longitudinal in character. This assumption was based upon the observation in both USb and UN that there was no critical scattering around the (0,0,1) magnetic Bragg peak position. At this position longitudinal critical scattering cannot be observed and the absence of critical scattering at (0,0,1) in the actinide systems was taken to mean that there was no transverse critical scattering.

We now believe, however, that there is an alternative explanation of this result in which the transverse critical scattering is not only nonzero, but diverges at the phase transition. This explanation is applicable to both single-$\mathbf{k}$ and triple-$\mathbf{k}$ structures, the latter of which may be thought of as the superposition of 3 single-$\mathbf{k}$ structures. At the (0,0,1) Bragg peak position in the single-$\mathbf{k}$ structure the Bragg peak structure factors for magnetic domains ordered with $\mathbf{k}=(1,0,0)$ and $\mathbf{k}=(0,1,0)$ are zero. The Bragg peak from the $\mathbf{k}=(0,0,1)$ domain cannot be observed at the (0,0,1) position because the neutron wave-vector transfer $\mathbf{Q}$ is parallel to the ordered magnetic moment (only spin components perpendicular to Q contribute to the magnetic neutron scattering cross section), and similarly the longitudinal scattering from this domain cannot be observed. If the transverse critical fluctuations in the $\mathbf{k}=(0,0,1)$ domain were therefore to take the form of clusters of spins which reorient themselves into the $\mathbf{k}=(1,0,0)$ or (0,1,0) domains then these clusters would have zero structure factor at (0,0,1). These "cluster excitations" would also affect the longitudinal susceptibility, although it can be seen from the above arguments that the critical scattering from this type of excitation, either longitudinal or transverse, in any of the three domains would be unobservable at the (0,0,1) position.

The dynamics of these cluster excitations would be expected to be diffusive in nature, leading to an inelastic spectrum that peaked at zero frequency rather than at nonzero frequency. However, such cluster excitations, if only thermally activated, would be expected to be a major part of the inelastic magnetic response only very close to the phase transition, while the observed "diffusive" behavior in USb extends down to $0.75T_N$. An estimate of whether this effect could arise solely from thermal fluctuations can be obtained from a comparison with the anisotropic antiferromagnetic insulator MnF_2,[22] where spin-wave peaks in the transverse susceptibility can be observed at temperatures as high as $\sim 0.98T_N$. It therefore seems unlikely that the "localized model" for the low-temperature behavior of USb used by Halg and collaborators[10] can in any way account for this effect. Whether the damping mechanism from the f-d coupling model used to explain the low-temperature absence of spin waves in the UX compounds with small lattice parameters could account for this behavior in USb remains to be seen.

We now turn our attention to the properties of USb in the critical region. It was shown by Mukamel and Krinsky[23] that type-I fcc antiferromagnets with the single $k=(1,0,0)$ structure in which the ordered magnetic moment is parallel to $\mathbf{k}$ belong to the universality class of systems with three independent order parameters ($n=3$). This result applies to UN and a similar analysis leads to a value of $n=3$ for USb as well. This classification of the phase transitions in UN and USb has been recognized before[3] although its implications have not been fully explored. The significance of the value of

$n=3$ arises from the renormalization-group calculations of Brézin *et al.*,[24] who have shown that for values of $n \leq 3$ the critical properties of a system should be independent of anisotropy in the Hamiltonian and should only depend on the values of d, the spatial dimension, and n, the number of independent order parameters. The best-known system in the $d=3$, $n=3$ universality class is the $d=3$ Heisenberg antiferromagnet, which is known to have both a divergent longitudinal and a divergent transverse susceptibility at the phase transition. The critical exponents for the $d=3$ Heisenberg antiferromagnet are $\nu_x=\nu_y=0.70$, $\gamma=1.38$,[25] and $\Delta=1.5$,[20] which are similar to those given in Table III for ν_x, ν_y, and Δ but substantially different to the value for γ. It is interesting to note that the value of $\gamma=1.74\pm0.15$ for USb is very close to the value of $\gamma\sim1.75$ obtained by Holden *et al.*[18] for UN. We will return to this point shortly. In the earlier work on the critical scattering[11] in USb the focus was on the anisotropy in the correlation lengths, i.e., K_y/K_x, and our value for this ratio is in good agreement with Ref. 11. However, the values for ν and γ obtained previously were clearly wrong. This difference may be attributable to a lack of stoichiometry in the earlier sample, since T_N was also considerably different.

A problem that arises when comparing the critical properties of USb with those of the $d=3$ Heisenberg antiferromagnet is that the transverse susceptibility of the Heisenberg antiferromagnet is infinite at all temperatures below the Néel temperature.[26] This is because of the complete rotational isotropy of the Hamiltonian for the Heisenberg antiferromagnet. In USb the presence of anisotropy means that the transverse susceptibility must be finite at temperatures below the phase transition. Consequently, it is not possible to compare the critical amplitude ratios in Table III with any theoretical values for the $d=3$ Heisenberg antiferromagnet. This observation provokes a question as to the size of the critical region in USb over which Heisenberg critical properties would be expected to be applicable. If the phase transition is approached from below then the transverse susceptibilities of USb and the $d=3$ Heisenberg antiferromagnet only coincide at T_N, suggesting that the crossover to Heisenberg behavior only occurs strictly at T_N. Consequently, the observed value of γ may reflect a strong crossover from anisotropic to isotropic behavior rather than being an exponent characteristic of the isotropic behavior. Since the exponents ν_x, ν_y, and Δ are close to the Heisenberg values it must be assumed that the critical region for these properties is larger than for the susceptibilities.

The qualitative features of the crossover from anisotropic to isotropic behavior for $K_x(T)$, $K_y(T)$, and $\Gamma(\mathbf{0},T)$ can be estimated from Figs. 8 and 12 which show log-log plots of these parameters over large reduced temperature ranges below and above T_N, respectively. A surprising feature of these figures is the experimentally observed values far from T_N are *larger* than the values calculated by extrapolating from the critical region. It would normally be expected that far from the critical region a crossover to mean-field behavior (where the exponents ν_x, ν_y and Δ are smaller) would occur, and hence that the observed parameters would be smaller than the extrapolated values. This is, however, not the case in USb and it can be speculated that this reverse of the expected behavior is a result of the crossover from anisotropic to isotropic behavior. In practical terms this behavior means that the effect of including data from outside the critical region in an analysis of the critical exponents would lead to values for the exponents ν_x, ν_y, and Δ which were too large. This could perhaps explain the large value of $\nu_x=\nu_y=0.84=\pm0.06$ observed by Holden *et al.*[18] in UN, where the data analyzed was taken over the relatively large reduced temperature range of $0.02<t<0.35$.

This discussion of the critical and precritical behavior in USb has, by necessity, been speculative since there is not, to the authors' knowledge, any detailed theoretical work available in the literature on the way in which an anisotropic system with $n=3$ would be expected to crossover to isotropic behavior at T_N. Such theoretical work would be invaluable in understanding the critical properties of UX antiferromagnets. In the same sense it is unfortunate that there also are no experimental studies of anisotropic antiferromagnetic insulators with $n=3$ with which we can compare our USb results. This comparison would allow us to determine how much of the observed behavior in USb can be ascribed to "critical effects" and how much is due to the more complicated magnetic interactions in USb. We hope that this current work may stimulate such theoretical and experimental studies in the future.

VI. SUMMARY

The temperature dependence of the low-frequency magnetic response at small reduced wave vectors $\mathbf{q}$ in USb has been measured by inelastic neutron scattering over a range of temperatures from 12 up to 320 K. The quantitative behavior of this low-frequency magnetic response is anomalous as a function of temperature.

At low temperatures, the low-frequency magnetic response takes the form of dispersive resolution-limited spin waves with a zone-center gap of 1.5 THz. In the temperature range up to 80 K the effect of temperature on these spin waves is to increase their intrinsic frequencies while leaving the line shapes relatively sharp. This behavior is different to that of most ferromagnets and antiferromagnets where the effect of temperature is to decrease the intrinsic frequencies. Above 80 K the low-frequency spin waves become heavily broadened and by 160 K they have collapsed into a Lorentzian form centered on zero frequency. An analysis of the spin-wave line shapes in this temperature range suggests that the intrinsic spin-wave frequencies continue to increase with temperature in the same way as below 80 K and that the broadening is due to a damping mechanism. This spin-wave collapse occurs at a temperature of $0.75T_N$.

The line shape of the low-frequency magnetic scattering above 160 K can be well described by a single function which is the product of a Lorentzian in wave vector and a Lorentzian in frequency. The continuity of the

scattering as it evolves from a spin-wave form below 160 K to a critical scattering form above 160 K, and the need for only one fitting function above 160 K, suggests that the transverse and longitudinal susceptibilities at low frequencies are degenerate or almost degenerate above 160 K, and that both diverge at T_N. Previous experimental investigations of these UX systems (as well as for the isostructural Ce compounds) have led to the assumption that the transverse susceptibility near T_N is zero. We now believe that this is incorrect and have proposed a model of the critical fluctuations which is consistent with the experimental observations but which also contains a divergent transverse susceptibility at T_N.

In the critical region around the Néel temperature the inverse correlation lengths and characteristic frequency associated with the low-frequency magnetic scattering display power-law behavior as a function of the reduced temperature with critical exponents which are consistent with the phase transition being in the universality class of the $d=3$ antiferromagnet with cubic anisotropy. The critical exponent found for the staggered static susceptibility is, however, substantially different to the value for the $d=3$ Heisenberg antiferromagnet, although it is very similar to the value found in UN by Holden *et al.*[18]

Well above T_N there are significant magnetic correlations that do not appear to follow the predictions of mean-field theory. Consequently, the temperature range over which deviations from mean-field theory are significant is very large in USb.

ACKNOWLEDGMENTS

The crystal used in this work was supplied by O. Vogt and K. Mattenberger of Eidgenössische Technische Hochschule (ETH), Zurich to whom we express our thanks. We acknowledge many informative and helpful discussions with J. W. Cable, R. A. Cowley, B. D. Gaulin, R. M. Nicklow, and T. A. L. Ziman. The excellent technical assistance provided by T. L. Collins, S. P. King, and J. R. Weir in performing these experiments at Oak Ridge National Laboratory (ORNL) is also gratefully acknowledged. The work at ORNL was supported by the Division of Materials Science of the U.S. Department of Energy under Contract No. DE-AC05-84OR21400 with Martin Marietta Energy Systems Inc. One of us (W.G.S.) expresses his gratitude to the staff of Oak Ridge National Laboratory for the hospitality shown during his stay.

*Present address: Neutron Division, Rutherford Appleton Laboratory, Chilton, Didcot, Oxon OX11 0QX, United Kingdom.

†On leave from Institut-Laue-Langevin, 156X, 38042 Grenoble Cédex, France. Present address: Department of Physics, University of Keele, Staffordshire ST5 5BG, United Kingdom.

‡Present address.

[1]An extensive review of these properties is given in *Handbook on the Physics and Chemistry of the Actinides,* edited by A. J. Freeman and G. H. Lander (North-Holland, Amsterdam, 1984), Vol. 1; *ibid.*, Vol. 2.

[2]J. Rossat-Mignod, G. H. Lander, and P. Burlet, in *Handbook on the Physics and Chemistry of the Actinides,* Ref. 1, Vol. 1, p. 415.

[3]W. J. L. Buyers and T. M. Holden, in *Handbook on the Physics and Chemistry of the Actinides,* Ref. 1, Vol. 2, p. 239.

[4]G. H. Lander, W. G. Stirling, and O. Vogt, Phys. Rev. Lett. **42**, 260 (1979); G. H. Lander and W. G. Stirling, Phys. Rev. B **21**, 436 (1980).

[5]J. Jensen and P. Bak, Phys. Rev. B **23**, 6180 (1981).

[6]J. Rossat-Mignod, P. Burlet, S. Quezel, and O. Vogt, Physica **102B**, 237 (1980).

[7]T. M. Holden, W. J. L. Buyers, E. C. Svensson, and G. H. Lander, Phys. Rev. B **30**, 114 (1984).

[8]W. G. Stirling, G. H. Lander, and O. Vogt, Physica **102B**, 249 (1980); M. Loewenhaupt, G. H. Lander, A. P. Murani, and A. Murasik, J. Phys. C **15**, 6199 (1982).

[9]T. M. Holden, W. J. L. Buyers, P. de V. DuPlessis, K. M. Hughes, and M. F. Collins, J. Magn. Magn. Mater. **54-57**, 1175 (1985).

[10]B. Halg and O. Vogt, J. Magn. Magn. Mater. **52**, 410 (1985); B. Halg and A. Furrer, Phys. Rev. B **34**, 6258 (1986).

[11]G. H. Lander, S. K. Sinha, D. M. Sparlin, and O. Vogt, Phys. Rev. Lett. **40**, 523 (1978).

[12]B. R. Cooper, R. Siemann, D. Yang, P. Thayamballi, and A. Banarjea, in *Handbook on the Physics and Chemistry of the Actinides,* Ref. 1, Vol. 2, p. 435.

[13]S. W. Lovesey, *Theory of Neutron Scattering from Condensed Matter,* (Clarendon, Oxford, 1984), Vols. 1 and 2.

[14]See, for example, J. W. Cable, R. M. Nicklow, and N. Wakabayashi, Phys. Rev. B **32**, 1710 (1985).

[15]See, for example, R. A. Cowley, W. J. L. Buyers, P. Martel, and R. W. H. Stevenson, J. Phys. C **6**, 2997 (1973).

[16]See, for example, G. F. Mazenko, in *Correlation Functions and Quasiparticle Interactions in Condensed Matter,* edited by J. W. Halley (Plenum, New York, 1978).

[17]J. Als-Nielsen, J. D. Axe, and G. Shirane, J. Appl. Phys. **42**, 1666 (1971).

[18]T. M. Holden, W. J. L. Buyers, E. C. Svensson, and G. H. Lander, Phys. Rev. B **26**, 6227 (1982).

[19]B. I. Halperin, P. C. Hohenberg, and S. K. Ma, Phys. Rev. B **10**, 139 (1974).

[20]P. C. Hohenberg, and B. I. Halperin, J. Appl. Phys. **41**, 1390 (1970).

[21]M. J. Cooper and R. Nathans, Acta Crystallogr. **23**, 357 (1967).

[22]M. P. Schulhof, R. Nathans, P. Heller, and A. Linz, Phys. Rev. B **4**, 2254 (1971).

[23]D. Mukamel and S. Krinsky, Phys. Rev. B **13**, 5065 (1976).

[24]E. Brézin, J. C. Le Guillou, and J. Zinn-Justin, Phys. Rev. B **10**, 892 (1974).

[25]S.-k. Ma, *Modern Theory of Critical Phenomena, Frontiers in Physics* (Benjamin, New York, 1976), Vol. 46.

[26]G. F. Mazenko, Phys. Rev. B **14**, 3933 (1976).